Optimizing Single-Breath Xenon Transfer Contrast MRI: Experimental Results, Theory, and Stochastic Modeling

Eric Frederick[1,2], Iga Muradian[3], Natalia Lisitza[3], Mike Dabaghyan[2], Mirko Hrovat[4], and Samuel Patz[3]

[1]*Brigham and Women's Hospital, Melrose, MA, United States,* [2]*Mirtech Inc.,* [3]*Brigham and Women's Hospital,* [4]*Mirtech, United States*

Introduction

Xenon Transfer Contrast (XTC) measures the rate of gas depolarization due to gas mixing between the dissolved and gas phases; providing information about gas exchange (1). As demonstrated by Ruppert, *et al.*, parameter optimization is essential (2). Using a single breath-hold XTC (SB-XTC) protocol, Patz *et al.* demonstrated the same information can be obtained with a single breath-hold of gas rather than the original two breath-hold protocol (3). This modification eliminates errors due to misregistration between image sets. It also reduces the number of images from 4 to 3 and the required amount of hyperpolarized gas.

In this work, we determined the optimal parameters for SB-XTC and compared our analytic results with experimental data as well as simulations. We found the optimal parameters for the SB-XTC protocol were different from (2) and we compared our data to those results. Unlike (2), we considered the effect of the number of phase encoding pulses. By halving (doubling) the in-plane resolution, we determined the minimum uncertainty is reduced (increased) by 82% (466%).

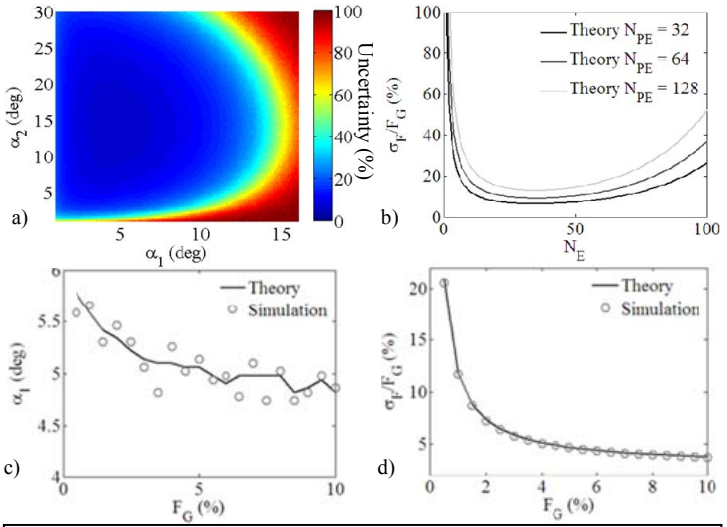

Figure-1a) Colormap of σ_F/F_G vs α_1 and α_2 for $N_E = 44$, $F_G = 2.5\%$, $D_G = 1\%$ depicting a local minimum along N_E. b) Plot of the local minima in σ_F/F_G vs. N_E for $F_G = 2.5\%$, $D_G = 1\%$ and different values of N_{PE}. Plots of c) optimal α_1 and d) global minimum in σ_F/F_G, versus F_G for $N_{PE} = 32$ and $D_G = 1\%$. Interestingly, α_2 was determined by N_{PE} and α_2 was 14 ± 0.5^o for the simulated results.

Theory

The SB-XTC MRI protocol generates contrast using a train of selective RF pulses applied at ∓200ppm with a fixed time between each excitation. The equations relating the signal intensities of the three images (S_1, S_2, and S_3) are:

$$S_1 \propto \rho \sin(\alpha_1)(\cos(\alpha_1))^{N_{PE}/2} \quad \text{Equation 1a)}$$

$$S_2 \propto S_1 \beta_1^{N_{PE}}(1-D_G)^{N_E} \quad \text{Equation 1b)}$$

$$S_3 \propto S_2 f_\alpha \beta_1^{N_{PE}+1-m}\beta_2^{m-1}\left[(1-D_G)(1-F_G)\right]^{N_E} \quad \text{Equation 1c)}$$

where ρ is the initial SNR density (arbitrary units (a.u.)·pixel^{-1}), $\beta_1 = [\cos(\alpha_1)\exp(-TR/T_1)]$, $\beta_2 = [\cos(\alpha_2)\exp(-TR/T_1)]$, $f_\alpha = \sin(\alpha_2)/\sin(\alpha_1)$, α_1 and α_2 are the flip angles for the images, N_{PE} is the number of phase encoding RF pulses, N_E is the number of inversions, D_G is the effective depolarization fraction due to T_1 relaxation and RF attenuation, and F_G is the effective depolarization rate due to gas mixing. The depolarization due to gas mixing (1) and relative measurement uncertainty (determined by error propagation and substitution) were calculated using:

$$F_G = 1 - \sqrt[N_E]{\frac{S_1 S_3}{S_2^2}\left(\frac{1}{f_\alpha}\left(\frac{\beta_2}{\beta_1}\right)^{m-1}\right)} \quad \text{Equation 2} \qquad \text{and} \qquad \frac{\sigma_F}{F_G} = \frac{1-F_G}{N_E F_G}\left[\frac{1}{SNR_1}\right]\left[1+\left[\frac{2}{\beta_1^{N_{PE}}(1-D_G)^{N_E}}\right]^2+\left[\frac{1}{f_\alpha \beta_1^{N_{PE}+1-m}\beta_2^{m-1}\left[(1-D_G)^2(1-F_G)\right]^{N_E}}\right]^2\right]^{\frac{1}{2}} \quad \text{Equation 3}$$

Methods

MRI experiments - A standard 2D gradient recalled echo (GRE) pulse sequence with no slice selection was used to acquire images from a single healthy volunteer. The data matrix was 64×32 with FOV = 30cm^2, TE = 6.6 ms, TR = 35.5 ms, and the flip angles were 3°, 3°, and 10° for the first, second, and third images, respectively. The number of contrast generating inversions varied from 10 to 54 and a total of eight data sets were acquired. The RF pulse width of each inversion was 10ms and each inversion was separated by 62ms. All images were reconstructed using Matlab.

Computer Simulations - Monte Carlo simulations were performed to verify Equation 3 using α_1 = 1–16°, α_2 = 1–30°, N_E = 1−100, N_{PE} = 32, 64, 128, D_G = 0.5−10%, and F_G = 0.5−10%. To ensure the simulations were comparable to the MRI data, we calculated the average SNR of the first image to be 65 a.u.·pixel^{-1}. Using this result, we estimated $\rho = 65/(\sin(3^o)\cos^{16}(3^o)) = 1{,}270 \approx 1{,}000$ a.u.·pixel^{-1}. We performed the Monte Carlo simulations using Equations 1a-c) by adding a different normally distributed pseudo-random number to each signal using Matlab's randn function with a mean of zero and a variance of one. Each simulation was repeated 16,384 times. We then generated histograms of F_G and calculated σ_F/F_G. For a given N_E, Matlab's min function was used to find the global minimum in σ_F/F_G.

Results

A colormap of σ_F/F_G for a given pair of flip angles is displayed in Figure1-a) to demonstrate the local minima along N_E. In Figure-1b), the global minimum in σ_F/F_G were 6.5%, 9.2%, and 13% for N_{PE} = 32, 64, and 128, respectively. In Figure-1c), the optimal choice for α_1 depended on F_G and our simulations indicate α_1 also depended on T_1, D_G, and N_{PE}. Interestingly, the optimal choice for α_2 depended only on N_{PE}. In Figure-2a), we observe an offset between the MRI data (black ⋆'s) and Equation-3. A similar offset is observed between Figure-2b) and the equation in (2). The offset between the predicted values and the data may be mostly due to physiological variations due to the observed gravitational gradient (2). We estimated these effects to be 11% using literature values (4).

Discussion

We compared our experimental data with Equation 3 and the equation reported in (2). While the concept of a finite magnetization reservoir is well-known, the initial SNR density was not considered in the previous study (2) and this observation allowed us to compare our results to the predicted values. From Figure-1b), we note the minimum uncertainty is reduced by 6.5/9.2 = 0.71 if N_{PE} is changed from 64 to 32. Because these plots used the same initial SNR density, we can account for the factor of 4 increase in SNR and estimate the uncertainty decreases by: $(1-(1/4)\cdot(0.71))\cdot 100\% = 82\%$. This concept and our stochastic modeling methodology may be an essential tool for pulse sequence design and quality assurance testing for hyperpolarized MRI studies.

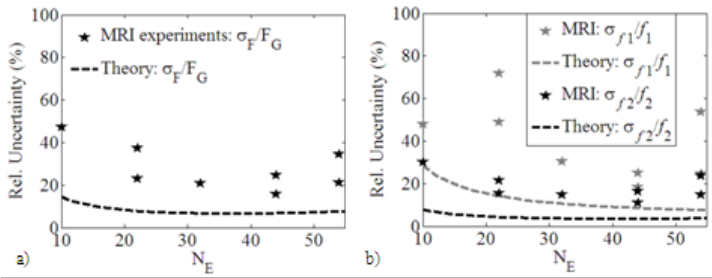

Figure-2. Relative uncertainty (⋆'s) for *in vivo* MRI experiments versus N_E. Dashed lines were created using Equation 3 with a) SNR_1 = 65 a.u.·pixel^{-1}, F_G = 2.15%, and D_G = 1% b) Equation reported in (2) with f_1 = 1.00%, SNR = 65 a.u.·pixel^{-1} and f_2 = 3.03%, SNR = 50a.u.·pixel^{-1}.

References

1.Ruppert K, *et al*. Magn Reson Med 2004;51(4):676-687. 2. Ruppert K, *et al*. Magn Reson Med 2007;57(6):1099-1109. 3. Patz S, *et al*. Eur J Radiol 2007;64(3):335-344. 4. Mercer RR, *et al*. J Appl Physiol 1994;77(3):1060-1066.